Journal of Catalysis 337 (2016) 133–137

Contents lists available at ScienceDirect

Journal of Catalysis

journal homepage: www.elsevier.com/locate/jcat

Correlation of Ti^{3+} states with photocatalytic enhancement in TiO_2-passivated *p*-GaAs

Jing Qiu [a], Guangtong Zeng [c], Mingyuan Ge [a], Shermin Arab [b], Matthew Mecklenburg [d], Bingya Hou [b], Chenfei Shen [a], Alexander V. Benderskii [c], Stephen B. Cronin [b,c,*]

[a] Department of Materials Science, University of Southern California, Los Angeles, CA 90089, USA
[b] Department of Electrical Engineering, University of Southern California, Los Angeles, CA 90089, USA
[c] Department of Chemistry, University of Southern California, Los Angeles, CA 90089, USA
[d] Center for Electron Microscopy and Microanalysis, University of Southern California, Los Angeles, CA 90089, USA

A R T I C L E I N F O

Article history:
Received 20 December 2015
Revised 31 January 2016
Accepted 1 February 2016

Keywords:
Photocatalysis
H_2 evolution
Energy conversion
GaAs
TiO_2
Solar fuel

A B S T R A C T

Recently, we reported enhanced H_2 evolution on TiO_2-passivated GaAs. Based on density functional theory (DFT) calculations, this enhancement was attributed to Ti^{3+} states, which bind reactant species and increase charge transfer across the semiconductor–liquid interface. Here, we provide a quantitative correlation between Ti^{3+} density, as measured by X-ray photoemission spectroscopy (XPS) and photoluminescence (PL) spectroscopy, and photocatalytic performance, which substantiates the hypothesis put forth previously. In the photo-*I*–*V* characteristics reported here, passivating GaAs with TiO_2 produces a shift in the onset potential of +0.35 V at 1 mA/cm^2 and enhances the photocurrent by 32-fold over bare GaAs (at 0 V vs. RHE), resulting in a peak photoconversion efficiency of 1.5% under AM1.5 G illumination. We find that just 1 nm of TiO_2 produces the best conditions for photocatalysis. XPS spectra show that thinner TiO_2 films (1 nm) have a higher density of Ti^{3+} states than thicker films (5 nm), which have lower photocatalytic performance. PL spectroscopy provides further evidence for these Ti^{3+} surface states, which cause increased surface recombination. While it is apparent that the TiO_2 films cause strong electron–hole recombination, the benefit that they provide by providing catalytically active sites outweighs their detriment associated with charge recombination. No enhancement is observed for TiO_2 thicknesses above 10 nm, which are crystalline and, therefore, considerably more insulating than thinner amorphous TiO_2 films.

© 2016 Elsevier Inc. All rights reserved.

Photocatalytic water splitting is of great interest for its potential to store solar energy in the form of chemical bonds that can later be released without producing harmful byproducts. In the initial demonstration of photocatalytic water splitting in 1972, Fujishima and Honda used TiO_2 under ultraviolet irradiation [1]. Because of TiO_2's wide band gap (E_g = 3.2 eV), however, very few solar photons (∼4%) can be used to drive this photocatalyst, and thus it will never provide efficient solar energy conversion on its own. Despite this inherent limitation, the low cost, easy synthesis and chemical robustness of TiO_2 have made it by far the most extensively studied photocatalytic material [2–5]. III–V compound semiconductors, such as GaAs and InP, are better candidate materials for solar utilization with band gaps of 1.42 eV and 1.34 eV, respectively. These band gap energies nearly match the Shockley–Queisser optimum band gap for solar energy conversion [6]. While the Shockley–Queisser limit is typically applied to electrical solar cells, its results are general and also apply to photocatalysts [7]. The long-standing record high applied-bias photon to current efficiency of 13.3% was obtained on *p*-type InP photocathodes covered with Pt catalysts [8]. More recently, Ali Javey's group reported 14% efficient H_2 evolution using InP nanopillars with a Ru catalyst [9]. While GaAs, a more widely used material, has a band gap and electron affinity that is similar to InP, it has not been reported to provide high efficiency solar-to-hydrogen conversion. One of the main reasons for this is the extremely high surface recombination velocity (10^6 cm/s) in GaAs, which is 1–2 orders of magnitude higher than most other III–V compound semiconductors. The rapid electron–hole pair recombination associated with this high surface recombination velocity lowers the overall efficiency of photocatalytic energy conversion [10–12]. Another major problem preventing GaAs from being utilized as a photocatalyst is that its surface is not photochemically stable, like other III–V semiconductors [13]. Several groups, including our own, have demonstrated that a very

* Corresponding author at: Department of Electrical Engineering, University of Southern California, Los Angeles, CA 90089, USA.

http://dx.doi.org/10.1016/j.jcat.2016.02.002
0021-9517/© 2016 Elsevier Inc. All rights reserved.

thin layer of TiO_2 can be used to make narrower band gap materials stable [9,14–22]. However, only Lin [23] and our groups' previous work [19–22,24] have reported an enhancement in the photoconversion efficiency due to the TiO_2-passivation layer, and the mechanisms of enhancement remain contradictory. In this paper, we correlate the Ti^{3+} states with photocatalytic activity using TEM, XPS, and PL spectroscopy. Also, in contrast to previous contributions by others, we investigate photocatalysts that do not contain metal co-catalyst particles, which allows us to study the semiconductor/liquid interface.

In this work, we deposit very thin layers of TiO_2 (1–5 nm) on GaAs by atomic layer deposition using $TiCl_4$ as the Ti precursor, and observe drastic enhancement in the photocatalytic efficiency compared to bare GaAs. We systematically investigate the photocatalytic performance as a function of TiO_2 thickness using gas chromatography and by measuring their photo-*I*–*V* characteristics as a function of reference potential. These photocatalytic surfaces are further studied using photoluminescence (PL) spectroscopy, high resolution transmission electron microscopy (HRTEM), electron energy-loss spectroscopy (EELS), and X-ray photoemission spectroscopy (XPS). To evaluate the photochemical stability of the TiO_2-passivated GaAs surfaces, we monitor the photocatalytic yield over 48 h under continuous illumination during the H_2 evolution reaction.

We use *p*-type (1 1 1) oriented GaAs substrates with a Zn dopant concentration of 6×10^{16} cm^{-3} (obtained from University Wafer, Inc.) as the photocathode for H_2 evolution. Atomic layer deposition (ALD) of TiO_2 was performed at 250 °C on the *p*-GaAs wafers using $TiCl_4$ as the titanium source and water vapor as the oxygen source. The carrier gas during the deposition was argon with a flow rate of 20 sccm, and $TiCl_4$ is always used for the first half-cycle. The thicknesses of TiO_2 were measured by ellipsometry. Ohmic back contacts were made to the *p*-GaAs by evaporating 1 nm thick Ti followed by 50 nm of Au. The Ti–Au film was then connected to the external circuitry with a copper wire and coated with epoxy cement to insulate it from the electrolytic solution, as illustrated in Fig. 1a. Fig. 1b shows a high resolution transmission electron microscope (HRTEM) image of 3 nm amorphous TiO_2 on GaAs below a layer of electron beam deposited Pt. Here, the Pt was deposited as part of the cross-sectional sample preparation using standard focused ion beam sample preparation techniques, and it was not used during the photoelectrochemical measurements. This high resolution TEM image confirms the thickness of the TiO_2 film, which was independently measured by ellipsometry. An HRTEM image of the GaAs surface prior to TiO_2 deposition is also shown in Fig. S2 in the Supplemental Document, which shows an approximately 3 nm native oxide on GaAs, consistent with the literature [25]. A scanning TEM (STEM) image and spatial maps of the Ti and O species obtained from EELS spectra are shown in Fig. S1 of the Supplemental Document. Based on these spatial maps, it is evident that the native oxide of the GaAs has been removed during the ALD process due to the Cl^- ions from the $TiCl_4$ precursor, consistent with previous reports in the literature values [25]. If there was a native oxide present, the oxygen EELS signal would increase before the titanium signal. Instead, the O and Ti EELS signals increase simultaneously, corresponding to the TiO_2 interface. We measured the photocatalytic reaction rates of two sets of samples in a pH = 0 solution of 0.5 M H_2SO_4 using a three-terminal potentiostat with the prepared samples, a Ag/AgCl electrode, and a graphite electrode functioning as the working, reference, and counter electrodes, respectively. A 910 mW/cm^2 532 nm laser and AM1.5 G illumination solar simulator (100 mW/cm^2) were used for illumination. The area of the exposed electrode surface was 0.2 cm^2. H_2 evolution was verified and quantified by gas chromatography. Photoluminescence spectra were collected using a 100× objective lens, a 1800 l/mm grating, and a silicon CCD detector. A 532 nm continuous-wave laser was used to excite the samples, and spectra were collected over the 750–1000 nm wavelength range. Low to moderate power excitation (10^2–10^5 mW/cm^2) was used to avoid optical heating.

Fig. 1c shows the photocurrent–voltage curves of *p*-GaAs photocathodes with various thicknesses of TiO_2 under an AM1.5 G illumination solar simulator, plotted together with bare GaAs. The bare GaAs (blue curve) exhibits an onset of photocurrent at a potential of approximately −0.05 V vs. RHE. The TiO_2-passivated GaAs shows a clear shift in the onset potential. The sample with a nominal thickness of 1 nm TiO_2 exhibits the most pronounced shift, lowering the overpotential (i.e., increasing the onset potential) by 0.35 V at 1 mA/cm^2 (red curve) with a 32-fold enhancement of photocurrent over bare GaAs (at 0 V vs RHE). It is interesting that such a large shift in the onset potential is obtained from such a thin layer of material. Nevertheless, these results were reproduced consistently in several different sets of samples. We observe no improvement over bare GaAs for TiO_2 thicknesses above 10 nm, which are crystalline, as shown in Fig. S3 of the Supplemental Document. This is because amorphous TiO_2 is far more conductive than crystalline TiO_2, which is insulating and, therefore, impedes charge transfer to the ions in solution [24]. The hydrogen evolution efficiency (η) was evaluated by computing the applied-bias photon to current efficiency of the photocatalytic reaction according to the following equation [26]

$$\eta = \left(\frac{(E_{\text{in}} - E_{\text{out}}) * I}{P_0}\right) 100\% \quad (1)$$

where E_{in} is the applied reference potential vs. RHE, E_{out} is the voltage of the redox couple (H^+/H_2) vs. RHE (which is 0 V in this case), I is the photocurrent density (mA/cm^2) observed, and P_0 is the incident optical power density (100 mW/cm^2). This equation gives the electrode efficiency for the H_2 evolution half-reaction [9,27]. The maximum applied-bias photon to current efficiency for *p*-GaAs with a 1 nm TiO_2 passivation layer reaches approximately 1.5% at an applied potential of +0.2 V vs. RHE, as shown in Fig. 1d. It should be noted that the photocatalysts measured in this study do not contain metal co-catalyst particles (typically consisting of precious metals), which are known to speed up the reaction kinetics. This allows us to explore the semiconductor/liquid interface, which has largely gone unstudied in these TiO_2/semiconductor heterojunctions. It is clear from these photo-*I*–*V* characteristics that the surface kinetics of the thinnest TiO_2 film (1 nm) provide the fastest kinetics. Our hypothesis is that this enhancement is due to a high density of Ti^{3+} defect states, which are more pronounced in the nominally 1 nm film. The light absorption by the 5 nm TiO_2 in visible range is negligible, and instead, we believe the reason for the slight decrease in performance seen for 5 nm films compared to 1 nm films is due to the defect density of the TiO_2 material which decreases with film thickness. In order to substantiate this claim, we have performed XPS spectroscopy and photoluminescence spectroscopy, as shown in Figs. 2 and 3, respectively.

Fig. 2 shows X-ray photoemission spectroscopy (XPS) of these TiO_2 deposited GaAs samples. Fig. 2a shows the core level binding energies of Ti $2p_{1/2}$ and Ti $2p_{3/2}$ in the TiO_2 film at 464.7 and 459.0 eV, respectively. Additional XPS peaks with lower binding energy of 457.1 eV (red fit curve) are assigned to Ti^{3+}. The area ratios of Ti^{3+} to Ti $2p_{1/2}$ are 0.15, 0.09, and 0.061 for the 1 nm, 3 nm, and 5 nm TiO_2 films, respectively, indicating a larger Ti^{3+} state density in thinner TiO_2 films. Fig. 2b shows the O 1 s core level peaks for samples with 1 nm, 3 nm, and 5 nm thick TiO_2 deposited on GaAs. Since the native oxide of the GaAs is removed during the ALD process, as is evident from the HRTEM data (see Fig. S1 of the supporting information), both O peaks in these XPS spectra are believed to originate from the TiO_2 thin layers. The O

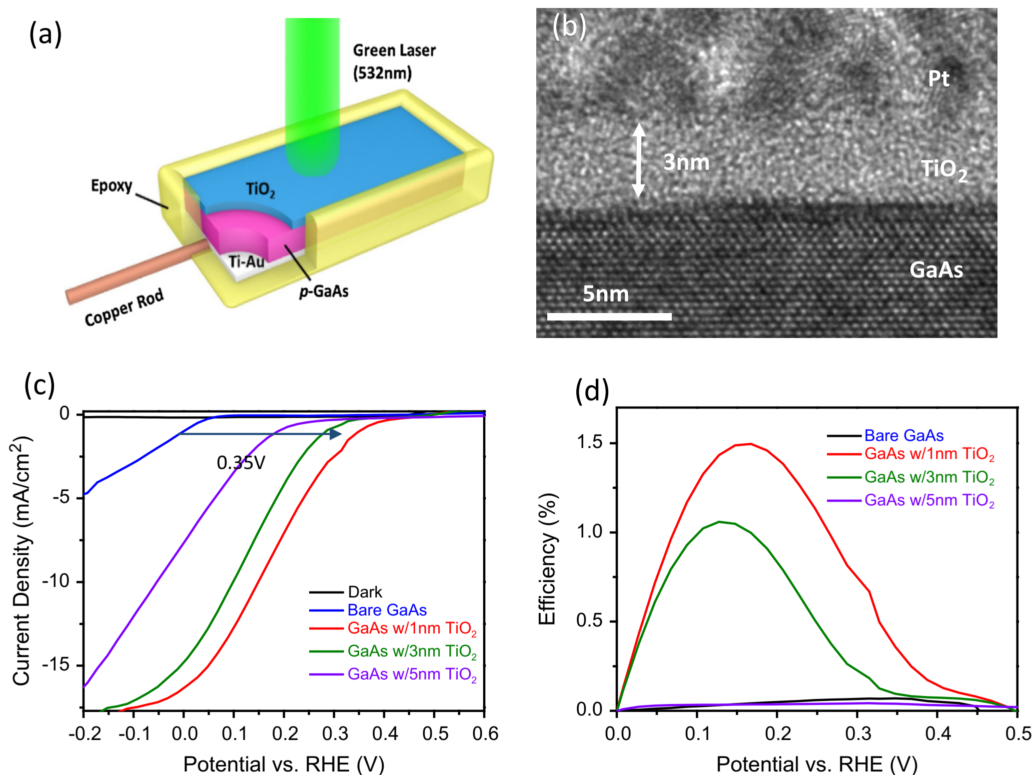

Fig. 1. (a) Schematic diagram of sample geometry. (b) TEM Image of 3 nm TiO_2 on GaAs. Note that for TEM sample preparation and imaging purposes, the surface of the substrate is coated with a thick layer of Pt. (c) Photocatalytic current–potential curves and (d) corresponding photon-energy conversion efficiency calculated by using Eq. (1) for GaAs photocatalysts with various thicknesses of TiO_2 under an AM1.5 G illumination in a 0.5 M H_2SO_4 pH = 0 solution.

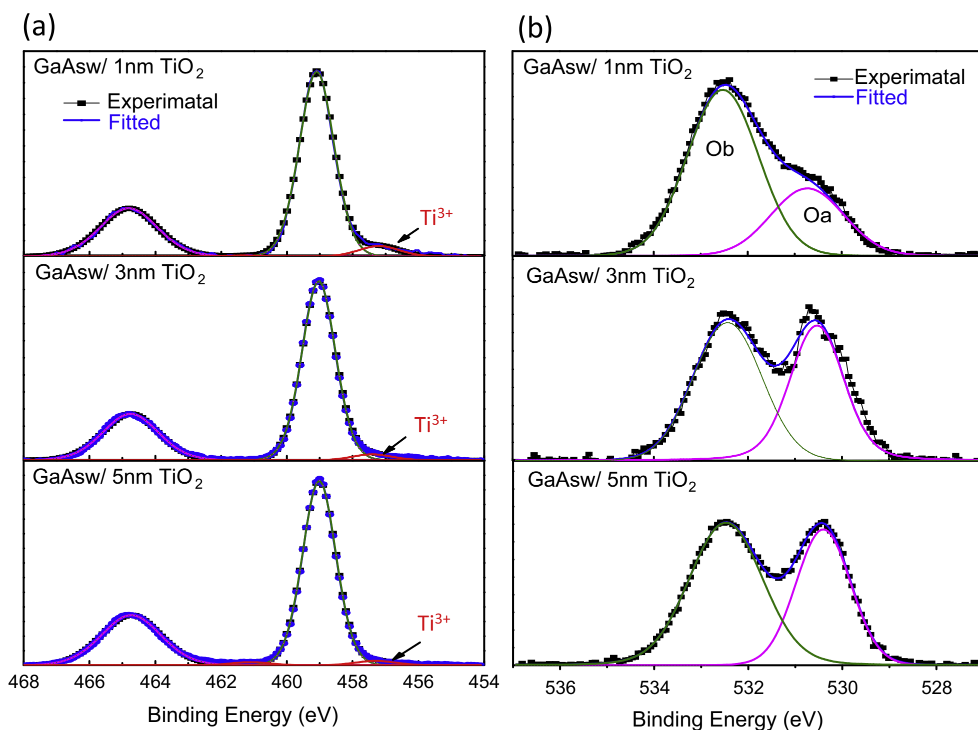

Fig. 2. (a) Ti 2*p* and (b) O 1*s* core level XPS spectra of various thicknesses of TiO_2 on GaAs.

1 s core level peaks are fitted with two symmetric Gaussian curves denoted as Oa and Ob. The Oa peak is ascribed to oxygen atoms of stoichiometric TiO_2 while the Ob peak corresponds to oxygen vacancies [28]. The area ratios of Ob to Oa are 2.4, 1.6, and 1.4 for the 1 nm, 3 nm, and 5 nm TiO_2 films respectively, indicating that the ratio of Ob to Oa decreases as the thickness increases. This implies that there are higher densities of oxygen vacancies in thinner TiO_2 films, which are consistent with the results of the Ti^{3+} XPS

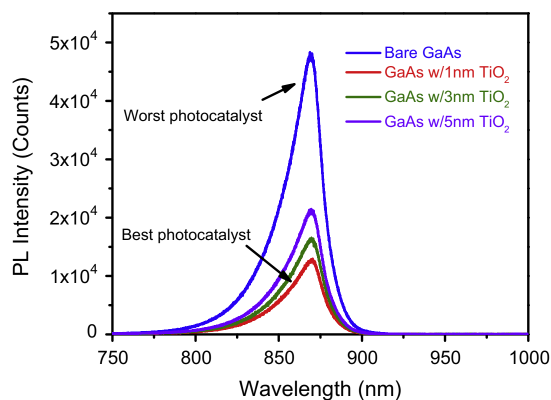

Fig. 3. Photoluminescence spectra of GaAs photocatalysts with various thicknesses of TiO_2 under 532 nm excitation.

peaks. Thus, a higher concentration of O vacancies corresponds to more active sites, resulting in a higher hydrogen generation efficiency and, hence, higher onset potentials. The dark *I–V* characteristics of TiO_2-passivated GaAs (Fig. S4 in the Supplemental Document) also show a large shift in the onset potential indicating that the catalytically active sites are primarily responsible for the enhanced H_2 evolution reaction. XPS data of GaAs with 3 nm TiO_2 passivation after a 12 h reaction (see Fig. S6 of the Supplemental Document) show the presence of Ti^{3+} peaks after the reaction.

In order to further explore the role of this TiO_2 (or TiO_{2-x}) surface layer, we also measured the photoluminescence (PL) spectra of these GaAs samples with various thicknesses of TiO_2. These spectra are plotted in Fig. 3. Here, we find that the sample with the highest PL efficiency (i.e., bare GaAs) has the lowest photocatalytic efficiency, and vice versa, and the sample with the lowest PL efficiency (1 nm TiO_2) has the highest photocatalytic efficiency. Initially, this was somewhat surprising, since materials with strong photoluminescence efficiencies typically make good solar cells and photocatalysts. However, it is apparent that the catalytically active surface states also cause strong electron–hole recombination, which limits the PL efficiency. However, the benefit that these surface states provide by lowering the potential barrier of the reaction and promoting charge transfer outweighs their detriment associated with charge recombination. For the sample with nominally 1 nm TiO_2, we observe a 5-fold reduction in the photoluminescence intensity (efficiency), indicating a high density of surface states, which act as non-radiative recombination centers, thus lowering the PL efficiency. GaAs with slightly thicker (3 nm and 5 nm) TiO_2 exhibits higher PL intensities than 1 nm TiO_2, by reducing the effects of these surface states. We have also seen this inverse correlation between PL intensity and photocatalytic activity for InP passivated with various TiO_2 thicknesses [21].

From thermodynamic considerations alone, GaAs (either *p*- or *n*-type) is known to be unstable under both anodic and cathodic conditions [29]. In our previous work on H_2 evolution on TiO_2-passivated GaP [30], atomic force microscopy (AFM) as well as photo-*I–V* characteristics showed that thin layers of TiO_2 protect the underlying GaP from corrosion in the strongly acidic electrolytic solution. We observe similar findings for TiO_2-passivated GaAs. Fig. S5a of the Supplemental Document plots the time dependent photocurrent of bare GaAs and TiO_2-passivated GaAs, which shows that bare GaAs corrodes readily while TiO_2-passivated GaAs is stable. We performed measurements extending over several hours monitoring H_2 evolution produced by GaAs coated with 3 nm TiO_2 under 532 nm wavelength illumination with an applied potential of +0.1 V (vs. RHE) in a 0.5 M H_2SO_4 solution. The yields of H_2 were measured by gas chromatography after 12, 24, and 48 h illumination times and are plotted in Fig. 4a. The H_2 peak appears at a GC retention time of 2.1 min, and the integrated area increases linearly with the illumination time. After calibration, the yields of H_2 in μmol were plotted as a function of time, as shown in Fig. 4b. The linear relationship of the H_2 yield versus time indicates that the TiO_2-passivated GaAs is photochemically stable in this strongly acidic electrolyte (pH = 0). Also, the time dependence of the photocatalytic current taken over a 48-h period is plotted in Fig. S5b of the Supplemental Document, which shows that this photocatalyst is stable over 48 h of illumination. The Faraday efficiencies of the 12, 24 and 48 h reactions are around 92%, as summarized in Table 1. We also measured the Faraday efficiency of bare GaAs to be only 6%, which is 15× lower than the TiO_2-passivated Faraday efficiency. This is most likely due to the photoelectrochemically-driven corrosion of the GaAs crystal structure that is circumvented by the TiO_2 layer.

In conclusion, we observe enhanced photocatalytic H_2 evolution on TiO_2-passivated GaAs. The TiO_2 layer hosts active surface states on the GaAs, which increases the recombination rate of photogenerated electron–hole pairs. The benefit of these active sites in lowering the potential barrier for this reaction outweighs the

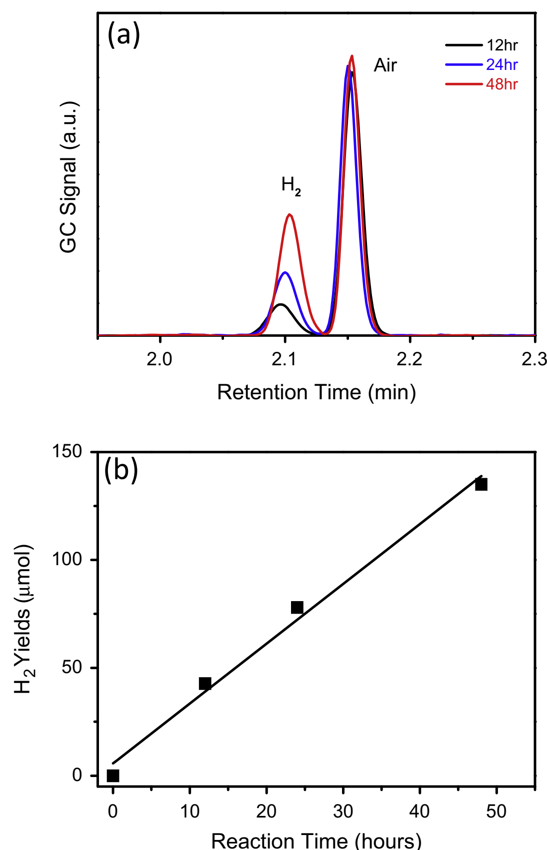

Fig. 4. (a) Gas chromatograph (GC) data taken after 12, 24, and 48-h reactions on GaAs with 3 nm TiO_2 under 532 nm illumination in a 0.5 M H_2SO_4 solution. (b) H_2 yield plotted as a function of time.

Table 1
H_2 yields and Faradaic efficiencies of the 12, 24, and 48-h reactions on GaAs with 3 nm TiO_2 under 532 nm illumination in a 0.5 M H_2SO_4 solution.

Reaction time (0.1 V vs. RHE) (h)	H_2 (μmol)	Faraday efficiency (%)
12	42.7	91.2
24	78	92.3
48	135	93.1

unfavorable effects of charge recombination, resulting in a net enhancement in the photocurrent density. The highest efficiency is obtained from GaAs with a 1 nm TiO_2 passivation layer under AM1.5 G illumination, which reaches 1.5% at an applied voltage of approximately +0.2 V vs. RHE. We observe no improvement over bare GaAs for TiO_2 thicknesses above 10 nm, where the insulating nature of the TiO_2 eventually outweighs its benefits. The TiO_2 passivation layer prevents photocorrosion of the GaAs surface, providing a viable, long-term stable photocatalyst. Moreover, the Faraday efficiency of TiO_2-passivated GaAs reaches 92%, 15× higher than that of bare GaAs which is only 6%.

Acknowledgments

This research was supported by ARO award No. W911NF-14-1-0228 (J.Q.), Air Force Office of Scientific Research Grant No. FA9550-15-1-0184 (G.Z.), and NSF Award No. CBET-1512505 (A. B.). XPS data were collected at the Molecular Materials Research Center of the Beckman Institute of the California Institute of Technology. Transmission electron microscope data presented in this article were acquired at the Center for Electron Microscopy and Microanalysis at the University of Southern California.

Appendix A. Supplementary material

Supplementary data associated with this article can be found, in the online version, at http://dx.doi.org/10.1016/j.jcat.2016.02.002.

References

[1] A. Fujishima, K. Honda, Nature 238 (5358) (1972) 37.
[2] A.K.L. Sajjad, S. Shamaila, B. Tian, F. Chen, J. Zhang, J. Hazard. Mater. 177 (1) (2010) 781–791.
[3] X. Wang, J.-G. Li, H. Kamiyama, Y. Moriyoshi, T. Ishigaki, J. Phys. Chem. B 110 (13) (2006) 6804–6809.
[4] M. Takeuchi, H. Yamashita, M. Matsuoka, M. Anpo, T. Hirao, N. Itoh, N. Iwamoto, Catal. Lett. 67 (2–4) (2000) 135–137.
[5] Z. Liu, W. Hou, P. Pavaskar, M. Aykol, S.B. Cronin, Nano Lett. 11 (3) (2011) 1111–1116.
[6] W. Shockley, H.J. Queisser, J. Appl. Phys. 32 (3) (1961) 510–519.
[7] R.T. Ross, J. Chem. Phys. 46 (12) (1967) 4590–4593.
[8] E. Aharon-Shalom, A. Heller, J. Electrochem. Soc. 129 (12) (1982) 2865–2866.
[9] M.H. Lee, K. Takei, J. Zhang, R. Kapadia, M. Zheng, Y.Z. Chen, J. Nah, T.S. Matthews, Y.L. Chueh, J.W. Ager, Angew. Chem. 124 (43) (2012) 10918–10922.
[10] R. Nelson, R. Sobers, J. Appl. Phys. 49 (12) (1978) 6103–6108.
[11] J. Lloyd-Hughes, S. Merchant, L. Fu, H. Tan, C. Jagadish, E. Castro-Camus, M. Johnston, Appl. Phys. Lett. 89 (23) (2006) 232102.
[12] C.-C. Chang, C.-Y. Chi, M. Yao, N. Huang, C.-C. Chen, J. Theiss, A.W. Bushmaker, S. LaLumondiere, T.-W. Yeh, M.L. Povinelli, Nano Lett. 12 (9) (2012) 4484–4489.
[13] K. Frese Jr., M. Madou, S. Morrison, J. Phys. Chem. 84 (24) (1980) 3172–3178.
[14] S. Hu, M.R. Shaner, J.A. Beardslee, M. Lichterman, B.S. Brunschwig, N.S. Lewis, Science 344 (6187) (2014) 1005–1009.
[15] Y.J. Hwang, A. Boukai, P. Yang, Nano Lett. 9 (1) (2008) 410–415.
[16] Y.W. Chen, J.D. Prange, S. Dühnen, Y. Park, M. Gunji, C.E. Chidsey, P.C. McIntyre, Nat. Mater. 10 (7) (2011) 539–544.
[17] K. Appavoo, M. Liu, C.T. Black, M.Y. Sfeir, Nano Lett. 15 (2) (2015) 1076–1082.
[18] X. Yang, R. Liu, C. Du, P. Dai, Z. Zheng, D. Wang, ACS Appl. Mater. Interfaces 6 (15) (2014) 12005–12011.
[19] J. Qiu, G. Zeng, M.-A. Ha, M. Ge, Y. Lin, M. Hettick, B. Hou, A.N. Alexandrova, A. Javey, S.B. Cronin, Nano Lett. 15 (9) (2015) 6177–6181.
[20] J. Qiu, G. Zeng, P. Pavaskar, Z. Li, S.B. Cronin, Phys. Chem. Chem. Phys. 16 (7) (2014) 3115–3121.
[21] G. Zeng, J. Qiu, B. Hou, H. Shi, Y. Lin, M. Hettick, A. Javey, S.B. Cronin, Chem. – Eur. J. 21 (39) (2015) 13502–13507.
[22] G. Zeng, J. Qiu, Z. Li, P. Pavaskar, S.B. Cronin, ACS Catal. (2014).
[23] Y. Lin, R. Kapadia, J. Yang, M. Zheng, K. Chen, M. Hettick, X. Yin, C. Battaglia, I.D. Sharp, J.W. Ager, J. Phys. Chem. C 119 (5) (2015) 2308–2313.
[24] J. Qiu, G. Zeng, M.-A. Ha, B. Hou, M. Mecklenburg, H. Shi, A.N. Alexandrova, S.B. Cronin, Chem. Mater. (2015).
[25] T. Gougousi, J.W. Lacis, Thin Solid Films 518 (8) (2010) 2006–2009.
[26] K. Shankar, J.I. Basham, N.K. Allam, O.K. Varghese, G.K. Mor, X. Feng, M. Paulose, J.A. Seabold, K.-S. Choi, C.A. Grimes, J. Phys. Chem. C 113 (16) (2009) 6327–6359.
[27] Z. Chen, T.F. Jaramillo, T.G. Deutsch, A. Kleiman-Shwarsctein, A.J. Forman, N. Gaillard, R. Garland, K. Takanabe, C. Heske, M. Sunkara, J. Mater. Res. 25 (01) (2010) 3–16.
[28] C. Rath, P. Mohanty, A. Pandey, N. Mishra, J. Phys. D Appl. Phys. 42 (20) (2009) 205101.
[29] S.-M. Park, M.E. Barber, J. Electroanal. Chem. Interfacial Electrochem. 99 (1) (1979) 67–75.
[30] J. Qiu, G. Zeng, P. Pavaskar, Z. Li, S.B. Cronin, Phys. Chem. Chem. Phys. 16 (2014) 3115.